Acta Crystallographica Section D
Biological Crystallography
ISSN 0907-4449

Structural characterization of *Spinacia oleracea* trypsin inhibitor III (SOTI-III)

Bernhard Glotzbach,[a]‡ Stefan Schmelz,[b]‡ Michael Reinwarth,[a] Andreas Christmann,[a] Dirk W. Heinz[b] and Harald Kolmar[a]*

[a]Institute for Organic Chemistry and Biochemistry, Technische Universität Darmstadt, Petersenstrasse 22, 64287 Darmstadt, Germany, and [b]Department of Molecular Structural Biology, Helmholtz Centre for Infection Research (HZI), Inhoffenstrasse 7, 38124 Braunschweig, Germany

‡ These authors contributed equally.

Correspondence e-mail: kolmar@biochemie-tud.de

Received 30 August 2012
Accepted 23 October 2012

PDB References: SOTI-III, wild type, complex with tryspin, 4aor; SOTI-III, F14A mutant, complex with tryspin, 4aoq

In recent decades, several canonical serine protease inhibitor families have been classified and characterized. In contrast to most trypsin inhibitors, those from garden four o'clock (*Mirabilis jalapa*) and spinach (*Spinacia oleracea*) do not share sequence similarity and have been proposed to form the new *Mirabilis* serine protease inhibitor family. These 30–40-amino-acid inhibitors possess a defined disulfide-bridge topology and belong to the cystine-knot miniproteins (knottins). To date, no atomic structure of this inhibitor family has been solved. Here, the first structure of *S. oleracea* trypsin inhibitor III (SOTI-III), in complex with bovine pancreatic trypsin, is reported. The inhibitor was synthesized by solid-phase peptide synthesis on a multi-milligram scale and was assayed to test its inhibitory activity and binding properties. The structure confirmed the proposed cystine-bridge topology. The structural features of SOTI-III suggest that it belongs to a new canonical serine protease inhibitor family with promising properties for use in protein-engineering and medical applications.

1. Introduction

Proteases and their natural inhibitors play key roles in biochemical and physiological processes. They are involved in protein digestion, defence mechanisms of plants, degradation and turnover of misfolded proteins, signalling, enzyme activation, regulation and many other processes (Antão & Malcata, 2005; Ehrmann & Clausen, 2004). Based on their reaction mechanism, proteases are basically categorized into serine proteases, cysteine proteases, aspartic proteases and metalloproteases. Protease activity has to be tightly controlled and two basic regulatory mechanisms have been described: the production of inactive precursors (Khan & James, 1998) and active inhibition by proteins, peptides or nonproteinaceous compounds (Clardy *et al.*, 2006; Krowarsch *et al.*, 2003). For the latter mechanism, the inhibitor blocks the active site of the proteolytic enzyme.

Serine protease inhibitors (SPIs) are classified based on their mode of inhibition as either canonical inhibitors, noncanonical inhibitors or serpins (Krowarsch *et al.*, 2003; Otlewski *et al.*, 1999). Serpins form an irreversible covalent enzyme–inhibitor complex, causing large conformational changes of the enzyme and thus disrupting the active site (Stubbs *et al.*, 1990; Silverman *et al.*, 2001). In contrast, the noncanonical inhibitors, such as hirudin, bind with their N-terminus *via* two interaction regions (Huntington & Carrell, 2001). This results in two-step kinetics, mainly owing to a substrate mimic in the active site and an additional exosite binding on the surface of the protease (Farady *et al.*, 2008).

Canonical inhibitors with a size of 3–21 kDa per domain obstruct the active site with a single convex inhibitor loop without causing conformational changes (Bode & Huber, 2000). The SPI P_1 residue is essential for complex formation and has a substantial influence on the association energy (Lu *et al.*, 1993).

From a structural point of view, there are various types of serine protease inhibitors such as α-helical proteins, β-sheet proteins, α/β proteins and small disulfide-rich proteins with different folds. While the serpin superfamily shares a highly ordered α_1-antitrypsin motif (Huber & Carrell, 1989; Loebermann *et al.*, 1984), the noncanonical SPIs have no well defined structural motif. However, they share a disordered N-terminal region that forms a parallel β-sheet with the protease upon complex formation (Otlewski *et al.*, 1999). Some canonical serine protease inhibitors, such as the BPTI, Kazal, potato, cereal, SSI, STI and ecotin families, have typical secondary-structure elements and a conserved hydrophobic core. Others, such as squash, Bowman–Birk, grasshopper and *Ascaris* inhibitors, lack this hydrophobic core, but maintain a defined tertiary structure, which is mainly formed and stabilized by intramolecular disulfide bonds (Krowarsch *et al.*, 2003; Bateman & James, 2011).

Among these, members of the cystine-knot miniprotein or knottin family show extraordinary chemical, thermal and proteolytic stability owing to their unique disulfide linkage (Kolmar, 2009; Heitz *et al.*, 2008; Werle *et al.*, 2008). Knottins are broadly distributed in nature and can be isolated from various organisms such as arthropoda, mollusca, porifera, vertebrata, fungi and plants (Kolmar, 2009). They act as ion-channel blockers (Williams *et al.*, 2008) and protease inhibitors (Avrutina *et al.*, 2005), and have insecticidal (Jennings *et al.*, 2001), antimicrobial (Tam *et al.*, 1999), anti-HIV (Gustafson *et al.*, 2004) or haemolytic activity (Daly *et al.*, 1999). Several studies have shown that the length of the loop, as well as its residue composition, can be modified as long as the cysteine pattern is preserved (Avrutina *et al.*, 2005; Kimura *et al.*, 2011; Sommerhoff *et al.*, 2010). Owing to their small size, their long-term stability and their likely oral availability, they are promising candidates for diagnostic and therapeutic applications (Kolmar, 2010; Werle *et al.*, 2008; Kimura *et al.*, 2011).

In 2007, a new family of serine protease inhibitors with a knottin-like disulfide-bridge connectivity of CysI–CysIV, CysII–CysV and CysIII–CysVI were described (Kowalska *et al.*, 2007). Based on their unique sequence and the C-terminal location of the inhibitor loop, these SPIs were proposed to form the new *Mirabilis* SPI family (http://knottin.cbs.cnrs.fr/; Fig. 1). Unfortunately, no subsequent new publication with additional information or a more detailed description of this family has been reported to date.

Figure 1
Sequence comparison of the squash (top) and *Mirabilis* (bottom) serine protease inhibitor families. Cysteine connections are not shown for the sake of clarity. Light gray, inhibitory active loop of the compared inhibitors; dark gray, P_1 residue of the inhibitors.

2. Materials and methods

2.1. Synthesis of linear precursors and oxidative folding

Peptides were assembled on Fmoc-Gln preloaded TentaGel resin (Rapp Polymere) using standard Fmoc-SPPS chemistry on a fully automated microwave CEM Liberty peptide synthesizer (see Supplementary Material[1]). Cleavage from the solid support was performed using 94%(*v*/*v*) TFA, 2%(*v*/*v*) H_2O, 2%(*w*/*v*) DTT, 1%(*v*/*v*) triethylsilane, 1%(*v*/*v*) anisole. After precipitation of the crude peptide in methyl-*tert*-butyl ether (MTBE), the pellet was washed twice with MTBE, dried, dissolved in a mixture of acetonitrile and water [1:4(*v*:*v*)], lyophilized, and finally analyzed by RP-HPLC and LC-MS (see §2.2). Oxidative folding was performed as reported previously (Avrutina *et al.*, 2005) followed by RP-HPLC purification.

2.2. RP-HPLC and LC-MS analysis

Analytical RP-HPLC was performed with a Varian LC 920 system equipped with a Phenomenex Synergi 4µ Hydro-RP 80 Å (250 × 4.6 mm, 4 µm) column (see Supplementary Material) at a flow rate of 1 ml min^{-1}. Semi-preparative RP-HPLC was performed with a Varian LC 940 system equipped with an Axia-packed Phenomenex Luna C18 (250 × 21.2 mm, 5 µm, 100 Å) column using linear acetonitrile gradients (Supplementary Material) with a flow rate of 18 ml min^{-1}.

LC-MS was performed with a Shimadzu LC-MS 2020 equipped with a Phenomenex Jupiter C4 (50 × 1 mm, 5 µm, 300 Å) column using linear acetonitrile gradients with a flow rate of 0.2 min^{-1} (Supplementary Material).

2.3. Crystallization and data collection

Trypsin from bovine pancreas (Sigma–Aldrich) was dissolved in 1 m*M* HCl pH 2.0, 10 m*M* $CaCl_2$. The protein was purified on a Superdex 75 16/60 column (GE Healthcare) in 25 m*M* MES pH 5.5, 50 m*M* NaCl, 10 m*M* $CaCl_2$ at 277 K and was concentrated to 12 mg ml^{-1}. Prior to crystallization setup, lyophilized SOTI-III was added to 12 mg ml^{-1} trypsin (in 25 m*M* MES pH 5.5, 50 m*M* NaCl, 10 m*M* $CaCl_2$) to a final concentration of 2.5 m*M* and kept on ice for 30 min. Initial crystallization screening was performed in Intelli-Plate 96-3

[1] Supplementary material has been deposited in the IUCr electronic archive (Reference: CB5019). Services for accessing this material are described at the back of the journal.

plates (Art Robbins) using a HoneyBee 961 dispensing robot (Digilab Genomic Solutions). Initial crystals were obtained with the JCSG+ screen (NeXtal; Qiagen) in condition E12 [tube 60; 0.1 *M* imidazole pH 8.0, 10%(*w*/*v*) PEG 8000]. Diffraction-quality crystals were obtained after several days at 292 K by mixing equal volumes of protein-complex solution with precipitant solution [0.1 *M* imidazole pH 7.5, 12%(*w*/*v*) PEG 8000] by hanging-drop vapour-diffusion crystallization in 15-well plates (EasyXtal; Qiagen) with a reservoir volume of 500 µl. Prior to flash-cooling in liquid nitrogen, the crystals (>0.8 × 0.1 mm) were cryoprotected with 25%(*w*/*v*) glycerol.

For SOTI-III F14A–trypsin complex crystals, lyophilized miniprotein was added to 11.5 mg ml^{-1} trypsin to a final concentration of 1.5 m*M* and incubated for 30 min on ice. The best crystals were obtained directly in condition B3 of the initial JCSG+ screen [tube 15; 0.1 *M* Bicine pH 9, 20%(*w*/*v*) PEG 6000; NeXtal, Qiagen] with equal volumes of complex protein and precipitant solution. Crystals grew at 292 K after several days and were cryoprotected with 33%(*w*/*v*) glycerol prior to flash-cooling in liquid nitrogen. X-ray diffraction data were collected on BESSY synchrotron beamline MX-14.1. Data were indexed, integrated and scaled with the *XDS*/*XSCALE* package (Kabsch, 2010). Phases were obtained with *Phaser* (McCoy *et al.*, 2007) using trypsin coordinates (PDB entry 2xtt; Wahlgren *et al.*, 2011) as a search model. The coordinates were refined with *phenix.refine* (Adams *et al.*, 2004) and manually checked and corrected with *Coot* (Emsley & Cowtan, 2004). SOTI-III coordinates were manually built with *Coot*. The refined SOTI-III–trypsin complex structure was used as a molecular-replacement model for the SOTI-III F14A–trypsin complex. Figures and structure alignments were prepared using *PyMOL* (Schrödinger). Data and refinement statistics are summarized in Table 1.

Table 1
X-ray data-collection and refinement statistics.

Values in parentheses are for the highest resolution shell.

	SOTI-III wild-type –trypsin complex	SOTI-III F14A –trypsin complex
Data collection		
Space group	$P2_1$	$P2_1$
Unit-cell parameters (Å, °)	a = 49.4, b = 66.8, c = 108.9, $\alpha = \gamma$ = 90.0, β = 90.02	a = 48.5, b = 68.4, c = 109.8, $\alpha = \gamma$ = 90.0, β = 93.3
Resolution (Å)	32.0–1.7 (1.8–1.7)	19.9–2.0 (2.1–2.0)
R_{merge} (%)	8.1 (49.1)	14.5 (45.0)
$\langle I/\sigma(I)\rangle$	11.66 (2.85)	8.27 (2.90)
Completeness (%)	97.3 (93.7)	98.7 (98.5)
Multiplicity	3.8 (3.8)	3.2 (3.2)
Matthews coefficient V_M (Å^3 Da^{-1})	2.04	2.02
No. of molecules in unit cell (Z)	6	6
Refinement		
No. of reflections	75888	48006
R_{work}/R_{free} (%)	17.9/22.1	16.7/22.0
B factors (Å^2)		
Protein	16.7	11.0
SOTI-III	21.0	16.2
R.m.s. deviations		
Bond lengths (Å)	0.010	0.003
Bond angles (°)	1.30	0.83
Ramachandran plot (%)		
Residues in favoured regions	97.2	97.1
Outliers	0	0
MolProbity score/percentile	1.53/90th	1.49/97th
PDB code	4aor	4aoq

2.4. Enzymatic methods

Bovine pancreatic trypsin (Sigma–Aldrich) was active-site-titrated (Chase & Shaw, 1967; Jameson *et al.*, 1973) using 4-methylumbelliferyl guanidinobenzoate (MUGB; 1 µ*M*; Sigma–Aldrich) in reaction buffer [50 m*M* Tris–HCl, 150 m*M* NaCl, 0.01%(*v*/*v*) Triton X-100, 0.01%(*w*/*v*) sodium azide, pH 7.6].

The concentration of inhibitory active SOTI was determined assuming a 1:1 interaction of enzyme and inhibitor (Avrutina *et al.*, 2005; Pohlig *et al.*, 1996). Several inhibitor concentrations (0.05–1.5 µ*M*) were incubated with trypsin (0.2 µ*M*) for 30 min at room temperature. Subsequently, the residual activity was quantified over 5 min by monitoring the relative fluorescence of the hydrolyzed carbobenzoxy-L-arginine-7-amino-4-methylcoumarin (75 µ*M*; Sigma–Aldrich).

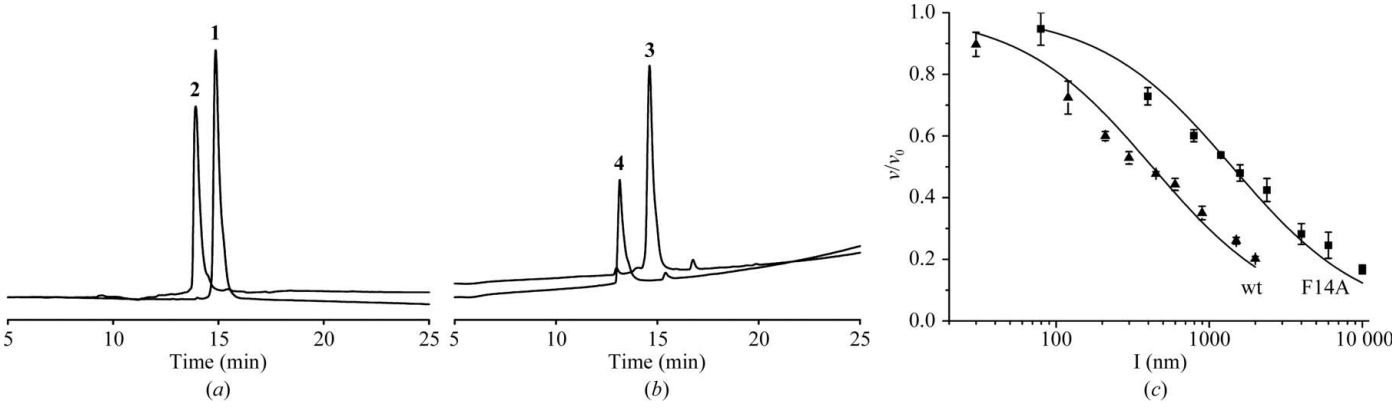

Figure 2
Oxidative folding of SOTI-III variants and inhibition curves of bovine pancreatic trypsin. (*a*) HPLC traces of wild-type linear precursor (**1**) and folded knottin (**2**) at 220 nm. (*b*) HPLC traces of F14A linear precursor (**3**) and folded knottin (**4**) at 220 nm. (*c*) The inhibition curves of SOTI-III (triangles) and SOTI-III F14A (squares) were obtained by fitting data to (1), as described in §2. Error bars were calculated from three independent experiments.

The reactions were carried out in 96-well microtiter plates (Greiner Bio-One, flat bottom, black) and were monitored in a Tecan GENios reader (excitation wavelength 360 nm, emission wavelength 465 nm). The normalized reaction rates were fitted using (1), with unfixed E_0. The ratio of active sites (see above) and the fitted E_0 gives a correction factor for the active inhibitor concentration.

To determine the inhibition constants, the reaction velocity was monitored after a 30 min pre-incubation of enzyme and inhibitor. The hydrolysis of the substrate Boc-QAR-pNA (250 µ*M*; Bachem) was analyzed over a period of 30 min at 405 nm (Tecan GENios). The apparent inhibition constant (K_i^{app}) was calculated by fitting (*SigmaPlot* 11; Marquard–Levenberg algorithm) the relative reaction velocities using the Morrison equation (1) (Morrison, 1969),

$$\frac{v}{v_0} = 1 - \frac{(E_0 + I_0 + K_i^{app}) - [(E_0 + I_0 + K_i^{app})^2 - 4E_0I_0]^{1/2}}{2E_0}. \quad (1)$$

All measurements were carried out in triplicate. The substrate-independent inhibition constants (K_i) were calculated from K_i^{app} and K_m of the enzyme using (2),

$$K_i = \frac{K_i^{app}}{\left(1 + \frac{[S]}{K_m}\right)}. \quad (2)$$

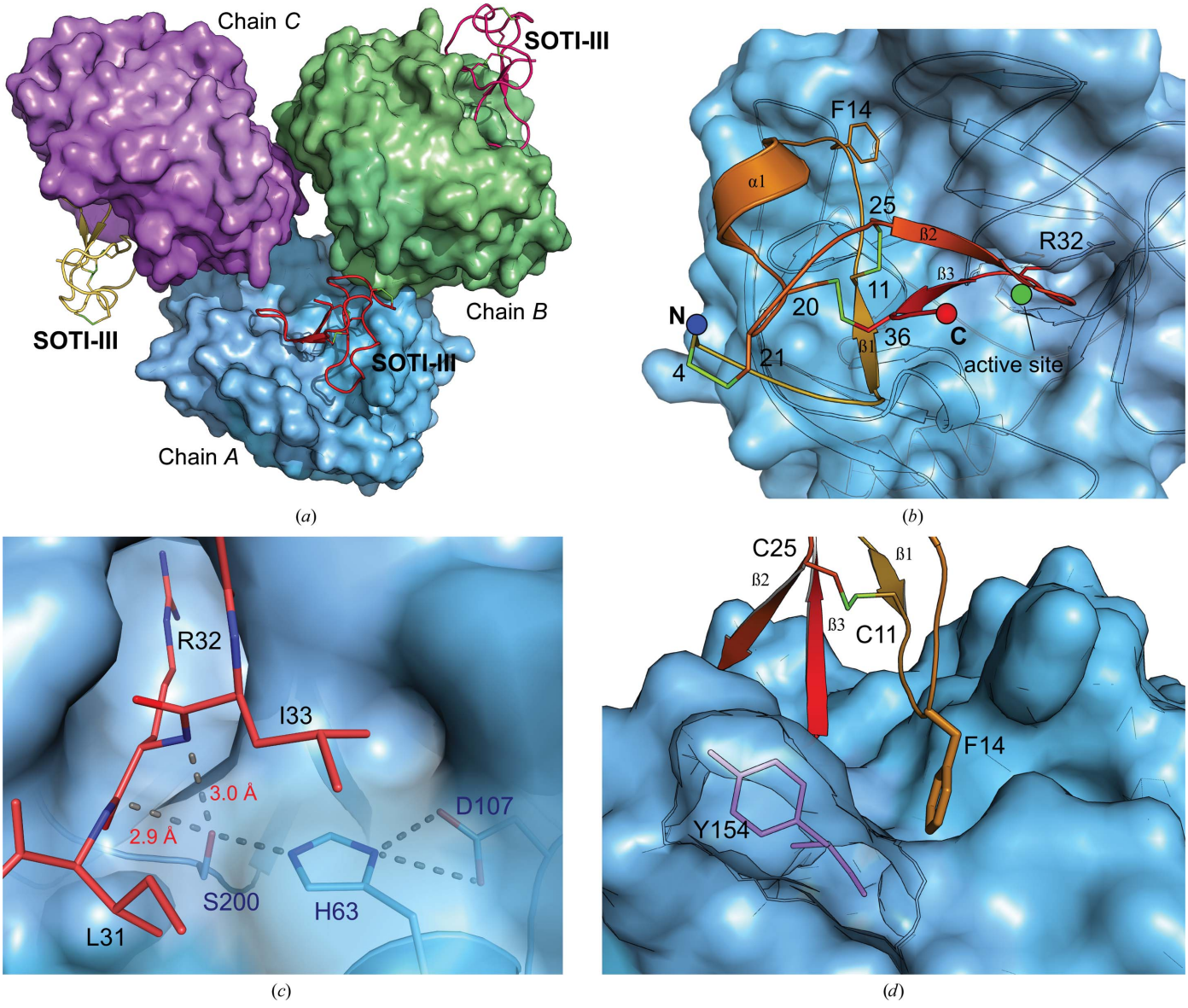

Figure 3
Structure of SOTI-III in complex with pancreatic trypsin. (*a*) Trimeric complex of trypsin (surface representation) with SOTI-III (cartoon representation) in the asymmetric unit. (*b*) SOTI-III binding pocket. Cysteine residues are colored green. Disulfide bonds are labelled with residue numbers. (*c*) Close-up of the SOTI-III inhibitor loop (red) blocking the catalytic triad (blue). Arg32 is coordinated in the S_1 pocket in a substrate-like fashion (Schechter & Berger, 1967). Dashed lines indicate hydrogen bonds. The closest hydrogen bonds of catalytic Ser200 to the inhibitor backbone are labelled in red. (*d*) Close-up of the subsite where Phe14 of SOTI-III is coordinated. Tyr154 of trypsin (purple) points away from residue 14.

The Michaelis–Menten constant K_m for the substrate and trypsin had been determined previously (Tischler *et al.*, 2012).

3. Results and discussion

3.1. SPPS and oxidative folding

SOTI-III and the F14A variant were synthesized by microwave-assisted solid-phase peptide synthesis (SPPS). The purity of the linear precursors was verified by HPLC (Fig. 2) and LC-ESI-MS analysis (Supplementary Fig. S1). Oxidative folding of the crude peptide was conducted in an aqueous buffer system and was monitored by analytical HPLC (Fig. 2) and LC-ESI-MS (Supplementary Fig. S1). After the final semi-preparative HPLC purification, total yields of 23.8% and 16.2% were obtained for SOTI-III and for the F14A variant, respectively.

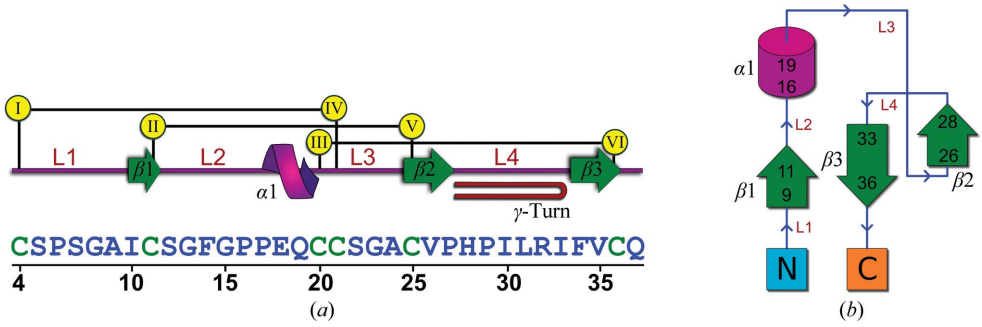

Figure 4
Secondary structure and topology of SOTI-III. (*a*) Secondary-structure elements of SOTI-III. The four loops (mainly β-turns) are labelled L1–L4. Green arrows indicate the three β-strands. The short helix α1 is colored purple. Disulfide bonds are drawn as black lines. The cysteine residues involved are labelled I–VI. The red U-shaped line symbolizes the β-hairpin with a γ-turn of the inhibitor loop L4. (*b*) Topology of SOTI-III. Residue numbers for boundaries of secondary-structure elements are shown. The coloring of secondary-structure elements is the same as in (*a*).

3.2. Structural studies

The crystals of the complex of purified SOTI-III with bovine pancreatic trypsin had $P2_1$ symmetry and diffracted to 1.7 Å resolution. The structure shows additional $F_o - F_c$ electron density for the inhibitor covering the active site of trypsin (Supplementary Fig. S2). The asymmetric unit is packed with three trypsin molecules, each blocked by the inhibitor (Fig. 3*a*). The SOTI-III secondary structure shows the proposed C4–C21, C11–C25 and C20–C36 disulfide linkages (Figs. 3*b* and 4*a*; Kowalska *et al.*, 2007). While the first cystine bridge is shaped as a right-handed hook, the second and last bridges form a right-handed and a left-handed spiral, respectively (Supplementary Table S1). The overall structure of the inhibitor is mainly constructed of β-turns (Fig. 4 and Supplementary Table S2). The turns are interrupted by disulfide bonds, three short antiparallel β-strands (residues 9–11, 26–28 and 33–36) and a short four-amino-acid-long helix (residues 16–19). The inhibitor loop (residues 26–34), which contains the S_1 site filled by Arg32 (P_1 residue), forms a β-hairpin with a γ-turn (Figs. 3*c* and 4 and Supplementary Table S2b).

SOTI-III coordinates at the active site of each trypsin molecule without causing major dislocation of the protease loops. Here, the average r.m.s.d. of 0.227 ± 0.026 Å for all three trypsin–inhibitor complexes in the asymmetric unit is in the same range as the r.m.s.d. of each trypsin–inhibitor complex when compared with apo trypsin (r.m.s.d. = 0.259 ± 0.008 Å; Supplementary Fig. S3). SOTI-III is most flexible in the regions of loop 1, loop 3 and a three-residue helix, as observed in a *B*-factor putty representation of all three monomers (Supplementary Fig. S4).

On average, 15 residues of the inhibitor (~750 Å^2) interact with 24 residues of trypsin covering ~980 Å^2 of the protease surface (Supplementary Table S3). A total of 12 hydrogen bonds are involved in coordination of the inhibitor. Notably, the P_1 residue Arg32 forms eight of these interacting hydrogen bonds (Supplementary Fig. S5).

Phe14 of SOTI-III binds to a cleft apart from the active site, which is formed by Ile78, Trp144 and Pro155 of trypsin (Fig. 3*d*). Interestingly, a detailed search in the Protein Data Bank showed that this cleft is not addressed by other trypsin inhibitors (Fig. 5; Supplementary Material).

To investigate the role of Phe14 upon trypsin binding and inhibition, a F14A variant of SOTI-III was synthesized and cocrystallized. The complex with F14A SOTI-III, which crystallized in the same $P2_1$ space group, shows that in monomer *C* of trypsin the residual space which was formerly filled by the side chain of Phe14 (Fig. 3*d*) is partly occupied by the protease residue Tyr154 (Supplementary Fig. S6). In one of the remaining two monomers the electron density is rather weak for the Tyr154 side chains, suggesting that the side chain might swap between those two rotamers.

The K_i values of wild-type SOTI-III and of the F14A variant were determined as described in §2. They were found to inhibit trypsin in the nanomolar range. The substrate-independent inhibition constants for SOTI-III and the F14A variant were calculated to be 60.9 ± 8.4 and 201.8 ± 27.7 n*M*, respectively, from the inhibition curves (Fig. 2*c*). This indicates that Phe14 contributes to trypsin binding. However, the main inhibitory effect is mediated by the C-terminal inhibitor loop. This is supported by the fact that more than half of the inhibitor-coordinating hydrogen bonds are formed by Arg32 within this loop region. This is not surprising, since other P_1 residues have also been reported to contribute strongly to inhibitor binding (Krowarsch *et al.*, 2005).

3.3. Comparison studies with other trypsin inhibitors

The structure of SOTI-III was previously modelled *in silico* (http://knottin.cbs.cnrs.fr/). Although the calculated structure is similar to that of the enzyme cocrystallized with trypsin, significant conformational differences are present in the C-terminal inhibitory loop region (residues 25–35). The

average r.m.s.d. of the superposed structure is 2.33 Å, with a largest r.m.s.d. of over 8 Å in the inhibitor loop region (Supplementary Fig. S7).

SOTI-III exhibits the unique, but well defined, pseudo-knot motif typical of members of the 'knottin' family (Figs. 3*b* and 4). This structural element determines the stability and rigidity, similar to the majority of known canonical protease inhibitors (squash, Bowman–Birk, grasshopper, hirustasin, chelonianin and *Ascaris* inhibitors) that lack a hydrophobic core and extensive secondary structure. It contains a canonical inhibitor loop located at the C-terminus, thereby defining it as a member of the huge family of canonical serine protease inhibitors.

The C-terminal location of the inhibitor loop is a unique feature of SOTI-III. Owing to the amino-acid sequence, the additional interaction of Phe14 and the location of the inhibitor loop, we support the notion of Kowalska *et al.* (2007) that SOTI-III together with other *Mirabilis* and

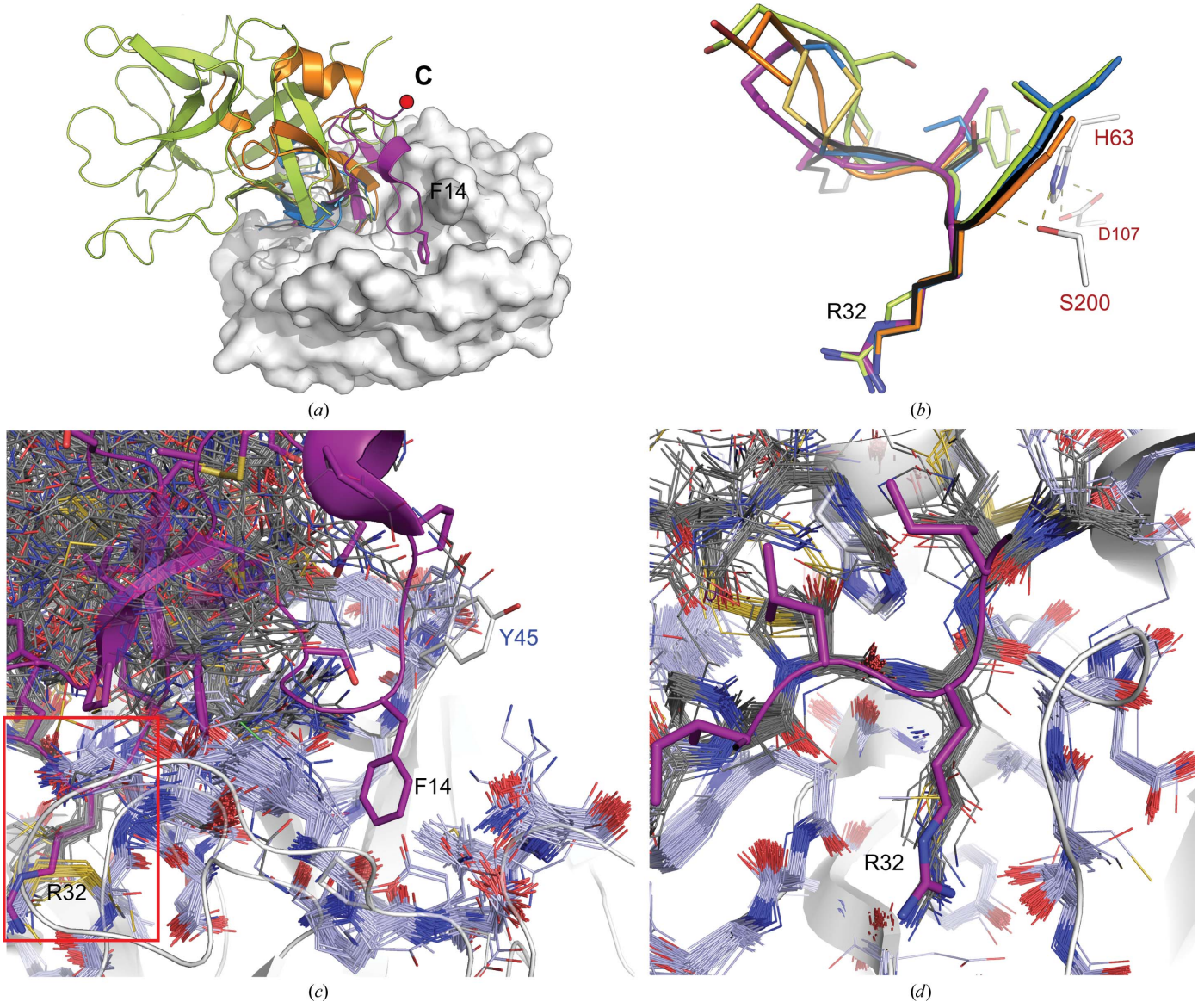

Figure 5
Comparison of the coordination of SOTI-III with those of other peptide trypsin inhibitors. (*a*) Superposition of SOTI-III with other canonical inhibitors. Trypsin is shown in surface representation. SOTI-III (chain *A*) is colored purple, STI lime (PDB entry 1avw; Song & Suh, 1998), SFTI-I black (PDB entry 1sfi; Luckett *et al.*, 1999), CPTI-II blue (PDB entry 2btc; Helland *et al.*, 1999) and BPTI orange (PDB entry 1f7z; Pasternak *et al.*, 2001). Inhibitors were superposed based on trypsin main-chain atoms. (*b*) Close-up of the active-site residues and the inhibitor loop with arginine or lysine P_1 residues. The coloring of the inhibitors is as in (*a*). Active-site residues are shown as sticks, with C, N and O atoms in white, blue and red, respectively. (*c*) Superposition with the SOTI-III complex of 99 deposited trypsin inhibitor structures that are close to residues 12–15 of SOTI-III in chain *D* (<3 Å; see Supplementary Material). SOTI-III is shown in purple and trypsin is shown in white. Superposed trypsin molecules (blue lines) align well, while the superposed inhibitors (gray lines) do not align or address the Phe14 binding site of SOTI-III. Tyr45 of trypsin in the SOTI-III complex has a different rotamer conformation. (*d*) Close-up of the inhibitor loop region in (*c*) showing the P_1 residue Arg32 (red box). The inhibitors superpose well with the SOTI-III inhibitor in this region.

Spinacia serine proteinase inhibitors form a new family of inhibitors.

This work was supported by Deutsche Forschungsgemeinschaft (DFG) through SPP1623 and Bundesministerium für Bildung und Forschung (BMBF).

References

Adams, P. D., Gopal, K., Grosse-Kunstleve, R. W., Hung, L.-W., Ioerger, T. R., McCoy, A. J., Moriarty, N. W., Pai, R. K., Read, R. J., Romo, T. D., Sacchettini, J. C., Sauter, N. K., Storoni, L. C. & Terwilliger, T. C. (2004). *J. Synchrotron Rad.* **11**, 53–55.

Antão, C. M. & Malcata, F. X. (2005). *Plant Physiol. Biochem.* **43**, 637–650.

Avrutina, O., Schmoldt, H.-U., Gabrijelcic-Geiger, D., Le Nguyen, D., Sommerhoff, C. P., Diederichsen, U. & Kolmar, H. (2005). *Biol. Chem.* **386**, 1301–1306.

Bateman, K. S. & James, M. N. G. (2011). *Curr. Protein Pept. Sci.* **12**, 340–347.

Bode, W. & Huber, R. (2000). *Biochim. Biophys. Acta*, **1477**, 241–252.

Chase, T. & Shaw, E. (1967). *Biochem. Biophys. Res. Commun.* **29**, 508–514.

Clardy, J., Fischbach, M. A. & Walsh, C. T. (2006). *Nature Biotechnol.* **24**, 1541–1550.

Daly, N. L., Love, S., Alewood, P. F. & Craik, D. J. (1999). *Biochemistry*, **38**, 10606–10614.

Ehrmann, M. & Clausen, T. (2004). *Annu. Rev. Genet.* **38**, 709–724.

Emsley, P. & Cowtan, K. (2004). *Acta Cryst.* D**60**, 2126–2132.

Farady, C. J., Egea, P. F., Schneider, E. L., Darragh, M. R. & Craik, C. S. (2008). *J. Mol. Biol.* **380**, 351–360.

Gustafson, K. R., McKee, T. C. & Bokesch, H. R. (2004). *Curr. Protein Pept. Sci.* **5**, 331–340.

Heitz, A., Avrutina, O., Le-Nguyen, D., Diederichsen, U., Hernandez, J. F., Gracy, J., Kolmar, H. & Chiche, L. (2008). *BMC Struct. Biol.* **8**, 54.

Helland, R., Berglund, G. I., Otlewski, J., Apostoluk, W., Andersen, O. A., Willassen, N. P. & Smalås, A. O. (1999). *Acta Cryst.* D**55**, 139–148.

Huber, R. & Carrell, R. W. (1989). *Biochemistry*, **28**, 8951–8966.

Huntington, J. A. & Carrell, R. W. (2001). *Sci. Prog.* **84**, 125–136.

Jameson, G. W., Roberts, D. V., Adams, R. W., Kyle, W. S. & Elmore, D. T. (1973). *Biochem. J.* **131**, 107–117.

Jennings, C., West, J., Waine, C., Craik, D. & Anderson, M. (2001). *Proc. Natl Acad. Sci. USA*, **98**, 10614–10619.

Kabsch, W. (2010). *Acta Cryst.* D**66**, 133–144.

Khan, A. R. & James, M. N. G. (1998). *Protein Sci.* **7**, 815–836.

Kimura, R. H., Jones, D. S., Jiang, L., Miao, Z., Cheng, Z. & Cochran, J. R. (2011). *PLoS One*, **6**, e16112.

Kolmar, H. (2009). *Curr. Opin. Pharmacol.* **9**, 608–614.

Kolmar, H. (2010). *Expert Rev. Mol. Diagn.* **10**, 361–368.

Kowalska, J., Pszczoła, K., Wilimowska-Pelc, A., Lorenc-Kubis, I., Zuziak, E., Ługowski, M., Łegowska, A., Kwiatkowska, A., Sleszyńska, M., Lesner, A., Walewska, A., Zabłotna, E., Rolka, K. & Wilusz, T. (2007). *Phytochemistry*, **68**, 1487–1496.

Krowarsch, D., Cierpicki, T., Jelen, F. & Otlewski, J. (2003). *Cell. Mol. Life Sci.* **60**, 2427–2444.

Krowarsch, D., Zakrzewska, M., Smalas, A. O. & Otlewski, J. (2005). *Protein Pept. Lett.* **12**, 403–407.

Loebermann, H., Tokuoka, R., Deisenhofer, J. & Huber, R. (1984). *J. Mol. Biol.* **177**, 531–557.

Lu, W., Zhang, W., Molloy, S. S., Thomas, G., Ryan, K., Chiang, Y., Anderson, S. & Laskowski, M. (1993). *J. Biol. Chem.* **268**, 14583–14585.

Luckett, S., Garcia, R. S., Barker, J. J., Konarev, A. V., Shewry, P. R., Clarke, A. R. & Brady, R. L. (1999). *J. Mol. Biol.* **290**, 525–533.

McCoy, A. J., Grosse-Kunstleve, R. W., Adams, P. D., Winn, M. D., Storoni, L. C. & Read, R. J. (2007). *J. Appl. Cryst.* **40**, 658–674.

Morrison, J. F. (1969). *Biochim. Biophys. Acta*, **185**, 269–286.

Otlewski, J., Krowarsch, D. & Apostoluk, W. (1999). *Acta Biochim. Pol.* **46**, 531–565.

Pasternak, A., White, A., Jeffery, C. J., Medina, N., Cahoon, M., Ringe, D. & Hedstrom, L. (2001). *Protein Sci.* **10**, 1331–1342.

Pohlig, G., Fendrich, G., Knecht, R., Eder, B., Piechottka, G., Sommerhoff, C. P. & Heim, J. (1996). *Eur. J. Biochem.* **241**, 619–626.

Schechter, I. & Berger, A. (1967). *Biochem. Biophys. Res. Commun.* **27**, 157–162.

Silverman, G. A., Bird, P. I., Carrell, R. W., Church, F. C., Coughlin, P. B., Gettins, P. G., Irving, J. A., Lomas, D. A., Luke, C. J., Moyer, R. W., Pemberton, P. A., Remold-O'Donnell, E., Salvesen, G. S., Travis, J. & Whisstock, J. C. (2001). *J. Biol. Chem.* **276**, 33293–33296.

Sommerhoff, C. P., Avrutina, O., Schmoldt, H.-U., Gabrijelcic-Geiger, D., Diederichsen, U. & Kolmar, H. (2010). *J. Mol. Biol.* **395**, 167–175.

Song, H. K. & Suh, S. W. (1998). *J. Mol. Biol.* **275**, 347–363.

Stubbs, M. T., Laber, B., Bode, W., Huber, R., Jerala, R., Lenarcic, B. & Turk, V. (1990). *EMBO J.* **9**, 1939–1947.

Tam, J. P., Lu, Y.-A., Yang, J.-L. & Chiu, K.-W. (1999). *Proc. Natl Acad. Sci. USA*, **96**, 8913–8918.

Tischler, M., Nasu, D., Empting, M., Schmelz, S., Heinz, D. W., Rottmann, P., Kolmar, H., Buntkowsky, G., Tietze, D. & Avrutina, O. (2012). *Angew. Chem. Int. Ed. Engl.* **51**, 3708–3712.

Werle, M., Kolmar, H., Albrecht, R. & Bernkop-Schnürch, A. (2008). *Amino Acids*, **35**, 195–200.

Wahlgren, W. Y., Pal, G., Kardos, J., Porrogi, P., Szenthe, B., Patthy, A., Graf, L. & Katona, G. (2011). *J. Biol. Chem.* **286**, 3587–3596.

Williams, J. A., Day, M. & Heavner, J. E. (2008). *Expert Opin. Pharmacother.* **9**, 1575–1583.